Seventh International Workshop on Power Definitions and Measurements under Non-Sinusoidal Conditions
Cagliari, July 10-12, 2006

Assessment of Fault Location in Power Distribution Networks

ALBERTO BORGHETTI, MAURO BOSETTI, MAURO DI SILVESTRO, CARLO ALBERTO NUCCI, MARIO PAOLONE, LORENZO PERETTO, ELISA SCALA, ROBERTO TINARELLI
Dipartimento Ingegneria Elettrica, Alma Mater Studiorum-Università di Bologna, Italy

Methods aimed at locating the position where a fault is occurred can be seen as part of a complex measurement system oriented at more general power quality purposes. This paper faces the comparison between two methods recently proposed in literature for fault-location in distribution networks. Making reference to a common distribution system topology, the two methods are applied in order to compare the obtained results and their performances. A possible integration of the two approaches is finally investigated and discussed.

1. Introduction

Increasing research interests are dedicated to the assessment of fault location in distribution power systems, as well as, more comprehensively, to detect and classify transient voltages according to their origin.
The problem of locating the source of faults has been extensively tackled in the literature, see e.g. [1-10]. The proposed methodologies can be grouped into three main categories: i) methods based on impedance measurement [1-3]; ii) methods based on the analysis of travelling waves [4-7]; iii) expert systems based on neural networks [8-10]. As far as methods i) are concerned, they essentially rely on the measurement of the fault impedance at power frequency, carried out by processing the voltage and current signals recorded in correspondence of the line terminals. Transmission lines are the typical application field of this technique: the line lengths and the simple network topology allow a good accuracy achievement. On the contrary, when the lines are short and the network has radial topology (as in distribution systems) methods ii) are usually preferred although they involve the adoption of more complex measurement and processing techniques. They rely on the analysis of the high-frequency components of voltages and currents during the fault. In this respect, wavelet-based analysis is often employed. Finally, the application of neural networks has been sometimes proposed; the required training stage can be performed also by means of a great number of simulations.
In this paper two methods for locating the source of faults are briefly reviewed and applied to the same distribution test network. Both methods can be considered belonging to category ii), even if their approaches are significantly different. The first method [11] is based on the use of a distributed measurement system: the source is located by measuring the starting instants of the transient originated by the fault in all the nodes of the monitored network, whose characteristics, with particular reference to its topology, must be known. The second one [12] is based on the use of the Continuous Wavelet Transform (CWT) to detect single frequencies that characterize the voltage transients generated by the fault. These frequencies can be used to infer the fault location, being the network topology and line conductor geometry, needed to determine the modal quantities of the multiconductor line, known.
The paper is organized as follows. Section 2 summarizes the main features of both the considered approaches. In Section 3, the considered test network and the relevant EMTP (Electromagnetic Transient Program) model are described. Finally, Section 4 compares the results and the performances achieved by using the two methods.

2. Considered approaches for fault location

In the following, the method based on the measurement of the transient starting instant and the method based on the use of the CWT will be referred to as method A and method B, respectively.

2.1 Method A

As briefly recalled in the previous Section, method A relies on a proper processing procedure of the starting instants of the voltage transients originated by the fault, measured in the monitored nodes of the network by using a distributed measurement system. Its proposed architecture is of master-slave type: a given number of slave units are located in all the nodes of the network. Each slave unit acquires both the starting instant and the waveform of the voltage transient. The former

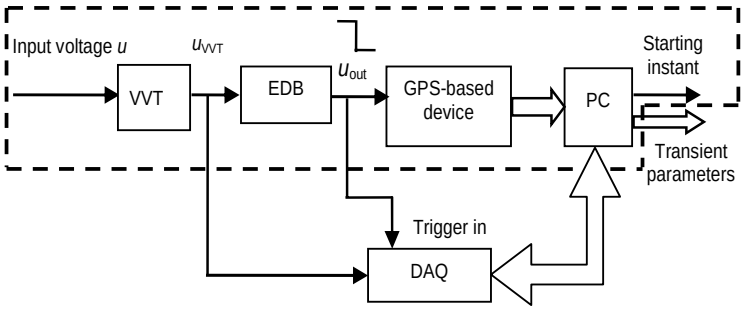

Figure 1 **Block diagram of a remote unit**

information is sent to the master unit, which locates the transient voltage source by relating the starting instants at all the slaves units to the stored characteristics of the network. Figure 1 shows the schematic block diagram of a slave unit: the dashed box contains the blocks performing the measurement of the transient starting instant. The voltage $u(t)$ at the monitored node is conditioned by a Voltage-to-Voltage Transducer (VVT), whose output u_{VVT} feeds an Event Detection Block (EDB). The EDB output u_{out} is a logic signal that, as a transient occurs, triggers both a Data AcQuisition board (DAQ) and a GPS-based device, which provides the relevant "time stamp". Figure 2 is the scheme of the operating principle implemented by the EDB [13]. First, the input signal u_{VVT} is low-pass filtered by the R_1-C_1 filter, which features a cut-off frequency of 1,600 Hz. This value allows the filter both to properly attenuate the transient affecting the transducer output and to make negligible the delay affecting the filter output u_+, due to the filter itself. u_{VVT} is also sent to the net C_2-R_a-R_b, which sums to u_{VVT} a negative bias provided by the trimmerable resistive divider R_a-R_b. Then, the operational amplifier compares the obtained signals: when $u_- > u_+$, a transient has occurred and the amplifier output must turn into the low level of a TTL signal. To this purpose, the high speed switching diode and the resistor R_2 are used to limit the low level of the comparator to 0 V. The falling edge of u_{out} is detected by a GPS-based device GPS168PCI. It provides the relevant time stamp with a resolution of 100 ns and a nominal accuracy of ± 250 ns.

Once the master unit has collected all the time stamps provided by the slave units, it applies a proper fault location procedure. To this purpose, it is assumed that: a) the network characteristics (topology, geometry, conductor spacing and type) are known; b) M slave units are installed in correspondence of each node of the network; c) the reference propagation interval between two adjacent nodes are known. Assumption a) does not appear a particular problem in practical cases. Assumption c) can also be fulfilled, for example, by carrying out proper EMTP simulations, for the various fault types.

The implemented procedure relies on the obvious concept that the larger the distant between the slave monitoring unit and the fault location, the greater the relevant time stamp value. Let us use the following notation:

t_{mk} time stamp of the starting instant of the transient voltage measured at the generic mth node ($1 \le m \le M$) on the kth phase ($k = a, b, c$ in the case of a three-phase network);

D_{nk} distance between two generic adjacent nodes, which form the nth couple ($1 \le n \le M$-1);

$T_{nk_{ref}}$, $T_{nk_{meas}}$ reference propagation time between two generic adjacent nodes and difference between the relevant measured time stamps, respectively.

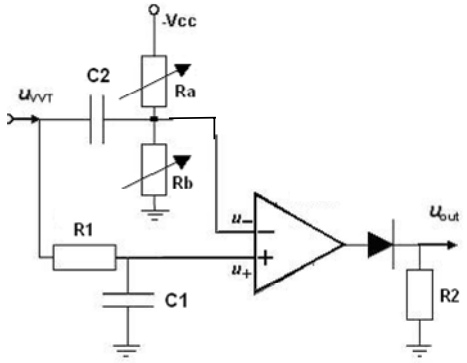

Figure 2 **Circuit implementing the event detection block (EDB)**

Due to the effects of various error sources, also for the case of a fault outside the line between the nth couple of nodes, $T_{nk_{meas}}$ may be different from the relevant $T_{nk_{ref}}$, being the former value always lower than the latter one when the fault is located within the line. A brief discussion on these error sources is reported in Section 4. The algorithm running on the master unit determines, for each phase and each couple of adjacent nodes, the quantity:

$$\Delta_{nk} = \frac{T_{nk_{ref}} - T_{nk_{meas}}}{T_{nk_{ref}}}, \qquad (1)$$

which ranges from zero to unity, depending on whether the fault is occurred outside or at the midst, respectively, of the considered line. Then, the algorithm seeks the maximum for Δ_{nk}, which we denote by $(\Delta_{nk})_{max}$. Such value identifies both the faulted phase and the couple of nodes within which the fault is occurred. Finally, the distance d between the fault location and the nearest node (which is the one identified by the lower time stamp) is determined by means of following relationship:

$$d = \frac{D_{nk}}{2}(\Delta_{nk})_{max} \qquad (2)$$

2.2 Method B

Method B relies on the fault voltage transients recorded, at least, in correspondence of one network bus. It is based on the application of the CWT on such a recorded transients. Let us briefly recall the main features of this transform. The CWT of a signal $s(t)$ is the integral of the product between $s(t)$ and the so-called daughter-wavelets, which are time translated and scale expanded/compressed versions of a function having finite energy $\psi(t)$, called mother wavelet. This process, equivalent to a scalar product, produces wavelet coefficients $C(a,b)$, which can be seen as "similarity indexes" between the signal and the so-called daughter wavelet located at position b (time shifting factor) and positive scale a:

$$C(a,b) = \int_{-\infty}^{\infty} s(t)\frac{1}{\sqrt{a}}\psi^*\left(\frac{t-b}{a}\right)dt, \qquad (3)$$

where * denotes complex conjugation.

Equation (3) can be expressed also in frequency domain [14]:

$$F(C(a,b)) = \sqrt{a}\psi^*(a\cdot\omega)S(\omega), \qquad (4)$$

where $F(C(a,b))$, $S(\omega)$ and $\psi(\omega)$ are the frequency-domain representation of $C(a,b)$, $s(t)$ and $\psi(t)$ respectively. Equation (4) shows that if the mother wavelet is a band-pass filter function in the frequency-domain, the use of CWT in the frequency-domain allows

for the identification of the local features of the signal. According to the Fourier transform theory, if the center frequency of the mother wavelet $\psi(\omega)$ is F_0, then the one of $\psi(a\omega)$ is F_0/a. Therefore, different scales allows the extraction of different frequencies from the original signal – larger scale values corresponding to lower frequencies – given by the ratio between center frequency and bandwidth. Opposite to the windowed-Fourier analysis where the frequency resolution is constant and depends on the width of the chosen window, in the wavelet approach the width of the window varies as a function of a, thus allowing a kind of time-windowed analysis, which is dependent on the values of scale a.

Several mother wavelets have been used in the literature (e.g. [15-20]). In this paper, the so-called Morlet wavelet is chosen as mother one $\psi(t)$:

$$\psi(t) = e^{-t^2/2} e^{j2\pi F_0 t} \tag{5}$$

CWT can operate at any scale, specifically from that of the original signal up to some maximum scale. CWT is also continuous in terms of shifting: during computation, the analyzing wavelet is shifted smoothly over the full domain of the analyzed function.

The CWT analysis is performed in time domain on the voltage transients recorded after the fault in a bus of the distribution network.

The analyzed part of the transient recorded signal $s(t)$, which can correspond to a voltage or current fault-transient, has a limited duration (few milliseconds, depending on the extension of the considered network) corresponding to the product between the sampling time T_s and the number of samples N. The numerical implementation of the CWT is obtained from (3) by substituting t and b with nT_s and iT_s, respectively:

$$C(a, iT_s) = T_s \frac{1}{\sqrt{|a|}} \sum_{n=0}^{N-1} \psi^* \left[\frac{(n-i)T_s}{a} \right] s(nT_s), \tag{6}$$

where $i = 0, 1, \ldots, N-1$. The signal energy $E_{cwt}(a)$, i.e. the sum of the squared values of all coefficients corresponding to the same scale,

$$E_{cwt}(a) = \sum_{n=0}^{N-1} C^2(a, nT_s) \tag{7}$$

identifies a 'scalogram' which provides the weight of each frequency component. By inspecting the relative maximum peaks of the obtained scalogram $E_{cwt}(a)$, the most significant frequency components of the signal are detected. Let us refer to these frequency components as 'CWT-identified frequencies' of the transient. The CWT-identified frequencies can be correlated to the propagation phenomena of the fault-originated waves, traveling along the lines, and to their reflections at discontinuity points.

A certain number P of paths covered by the traveling waves (and hence a certain number P of corresponding frequencies) can be associated to a given measurement point, depending on the number of line termination of the network. These theoretical frequencies can be determined a priori, providing the network topology and propagation speeds for the various fault types are known. When a fault occurs, the analysis of $E_{cwt}(a)$, obtained by processing the voltage signal acquired at the considered measurement point, provides P CWT-identified frequencies [12]. *P-1* frequencies are used to identify the faulted branch of the radial network and the remaining frequency to identify both the fault location in the faulted line (see section 4).

It is worth noting that the propagation of traveling waves in multiconductor transmission lines, involves the presence of different propagation speeds. Therefore, the CWT-based analysis is carried out separately for the various propagation modes [23] . Equations (8) and (9) show the so-called modal transformation, through transformation matrices $[T_e]$ and $[T_i]$ adopted for voltages and currents respectively.

$$\left[\frac{d^2 V^{ph}}{dx^2} \right] = [Z'][Y'][V^{ph}]$$
$$\left[\frac{d^2 I^{ph}}{dx^2} \right] = [Y'][Z'][I^{ph}] \tag{8}$$

$$[V^{ph}] = [T_e][V^m]$$
$$[I^{ph}] = [T_i][I^m] \tag{9}$$

$$\left[\frac{d^2 V^m}{dx^2} \right] = [\gamma]^2 [V^m]$$
$$\left[\frac{d^2 I^m}{dx^2} \right] = [\gamma]^2 [I^m] \tag{10}$$

where the *ph* and *m* denote phase and modal variables, Z' and Y' are the impedance and admittance matrix in per unit of length, $[\gamma]^2$ is the diagonal matrix of the common eigenvalues of products $[Z'][Y']$ and $[Y'][Z']$, being $\gamma_i = \alpha_i + j\beta_i$ the propagation constant of mode i, α_i the attenuation constant and β_i the phase constant of mode i. The phase velocity of mode i is given by:

$$v_i = \frac{\omega}{\beta_i} \tag{11}$$

Considering that multiconductor distribution lines are usually unbalanced, the calculation of the matrixes $[T_e]$ and $[T_i]$, which must be real in order to be adopted in a time-domain application of the CWT, is performed using EMTP.

The implementation of methods B does not require the use of a distributed system with a slave unit at each bus, although in complex and large distribution networks multiple measurement points would allow improved performances.

3. Application examples

Computer simulations have been carried out to compare both the considered approaches. EMTP-RV [21,22] has been used to simulate the transient response of a faulted distribution test network, whereas MATLAB scripts were developed in order to emulate all the instrumentation and processing devices required by the two methods.

Figure 3 shows the considered distribution test network. It is composed by a 10-km long main feeder (lines L1, L2 and L3) and by two laterals of 2-km length (L4) and 1-km length (L5). The overhead lines are assumed

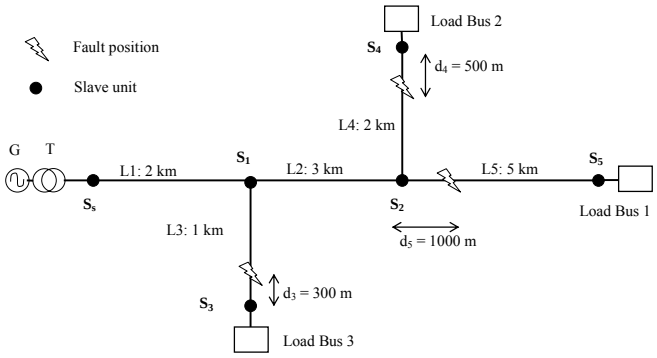

Figure 3 **The test network (not in scale)**

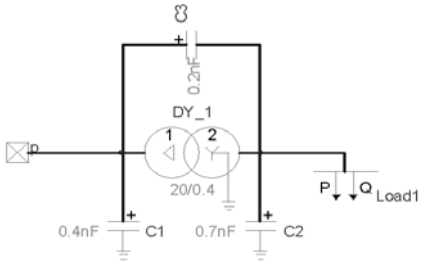

Figure 4 **Configuration of the load blocks**

balanced, therefore transformation matrixes $[T_e]$ and $[T_i]$ of equations (8) and (9) are identical and real, being the Clarke's (0,α,β) transformation matrix [23].

The power distribution network is fed through a 150/20 kV substation G, whose transformer T has a Yg/d connection.

Figure 4 illustrates the load blocks connected at bus 1, 2 and 3 of Figure 3. Each load is connected at the low voltage side of a 20/0.4 kV distribution transformer and it is represented by three impedances. A Π of capacitance is also included in parallel at each transformer model in order to simulate, in a first approximation, its response to transients at a frequency range around 100 kHz.

Phase-to-ground and three-phase short circuits have been simulated at three different locations, shown by flashes in Figure 3, by using ideal switches, closed at 1.5 ms. For the application of Method A, six slave units of the distributed measurement system are supposed to be placed in all the network nodes, shown by black bullets in the figure and denoted by S_s, S_1, S_2, S_3, S_4 and S_5. For Method B, the voltage transients are assumed to be recorded by unit S_s.

For method A, the simulation time step was set to 10 ns to grant the typical time resolution of an analog device such as the EDB of Figure 2. Method B has been applied by assuming 1 μs of simulation time step in order to emulate a 1 MSa/s sampling frequency of the DAQ. The values of $T_{nk_{ref}}$, required by method A, have been obtained by the simulation of the propagation of a voltage pulse injected at bus S_s

4. Results and discussion

The discussion of the results is here limited to the ones relevant to faults in line L3 and L5 (phase-to-ground and three phase short circuits) and can be straightforward applied to faults located in all the other branches of the considered distribution snetwork.

Table 1

Values of Δ_{nj} (p.u) in the case of fault in line L3

Nodes couples	Phase-to-ground fault			Three-phase fault		
	Δ_{na}	Δ_{nb}	Δ_{nc}	Δ_{na}	Δ_{nb}	Δ_{nc}
	($\cdot 10^{-2}$)			($\cdot 10^{-2}$)		
$S_s - S_1$	0.04	0.04	0.04	0.04	0.04	0.04
$S_1 - S_2$	0.14	0.14	0.14	0.14	0.14	0.14
$S_1 - S_3$	**60**	**60**	**60**	**60**	**60**	**60**
$S_2 - S_4$	0.04	-0.11	-0.11	0.04	-0.11	0.04
$S_2 - S_5$	0.04	0.04	0.04	0.04	-0.02	0.04

4.1 Faults in line L3

The fault location is 300 m away from the nearest node (bus S_3) and 2.7 km from S_s.

Table 1 shows the values of Δ_{nk} estimated for all the node couples and for both types of fault. In both this table and the following ones, the values of $(\Delta_{nj})_{max}$ are in bold characters. Line L3, defined by the slave units located in S_1 and S_3, is correctly identified as faulted. The application of (2) provides values of d equal to 300.1 m and 300.6 m for phase-to-ground and three-phase short circuit, respectively.

As far as method B is concerned, Figure 5 illustrates six paths covered by travelling waves originated by a fault in the line L3. The travelling waves are reflected at the line terminations and at the fault location. Paths with partial reflections at the point where more lines converged are here disregarded. Only three paths (namely paths 3, 1 and 2) reach the observation point, assumed at bus S_s.

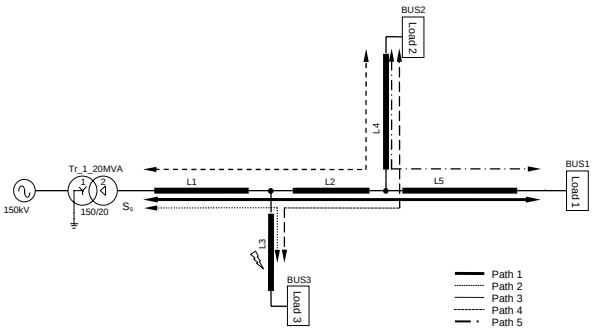

Figure 5 **Paths covered by travelling waves caused by a fault at line 3.**

As mentioned in section 2.2, it is possible to correlate each path to characteristic frequencies of the fault transient recorded at the observation point by the following considerations: path 3 is associated to a period given by a travelling time equal to 4 times L1+0.7*L3 divided by the propagation speed of the considered propagation mode (see equation (11)), as the travelling wave experience reflections of opposite sign at the fault location and at the sending end of the main feeder. For paths 1 and 2, the associated periods are given by the travelling time relevant to the double path lengths (L1+L2+L4 and L1+L2+L5, respectively), as the travelling wave is reflected at the line terminations.

The results of the CWT analysis of the propagation mode β relevant to the voltage transient due to a three phase

fault at line L3 observed in the node S_s produce the identified frequencies shown in Table 2 that reports also the fault distance error from bus S_s estimated on the identified frequency relevant to the path L1+0.7*L3. As can be seen such an error is of 249.2 m.

Table 2
Frequency values theoretically associated to the paths covered by the travelling waves of mode β, originated by a balanced three-phase fault at line L3, and values identified by the CWT analysis.

Path	Length (km)	Theoretical frequency value (traveling wave at light speed) (Hz)	CWT identified frequency value (kHz)	Fault distance error from bus S_s (m)
L1+0.7•L3	4•2.7	27.2	30.0	249.2
L1+L2+L4	2•7	21.0	19.6	
L1+L2+L5	2•10	14.7	14.7	

Table 3 presents the results of the CWT analysis of the propagation mode 0 relevant to the voltage transient due to a phase-to-ground fault at line L3 observed in the node S_s. For this case the fault location error is of 533.9 m.

Table 3
Frequency values theoretically associated to the paths covered by the travelling waves of mode 0 originated by a phase-to-ground fault at line L3, and values identified by the CWT analysis.

Path	Length (km)	Theoretical frequency value (traveling wave at light speed) (Hz)	CWT identified frequency value (kHz)	Fault distance error from bus S_s (m)
L1+0.7•L3	4•2.7	22.5	28.8	533.9
L1+L2+L4	2•7	17.3	14.0	
L1+L2+L5	2•10	12.1	8.8	

4.2 Faults in line L5

The fault location is 1000 m away from the slave unit S_2, located in the nearest node, and 5 km away from S_s. Table 4 reports the relevant values of Δ_{nk}. The line L5, defined by the slave units located in S_2 and S_5, is correctly identified as faulted. The application of (2) provides values of d equal to 1000.6 m for both phase-to-ground and three-phase short circuit.

Table 5 presents the results of the CWT analysis of the propagation mode β relevant to the voltage transient due to a balanced three-phase fault at line L5 observed in the node S_s. For this case the fault location error is of 553.7 m. In the case of phase-to-ground fault, Table 6 shows that the location error is 1261.7 m.

Table 4
Values of Δ_{nj} (p.u) in the case of fault in line L5

Nodes couples	Phase-to-ground fault			Three-phase fault		
	Δ_{na}	Δ_{nb}	Δ_{nc}	Δ_{na}	Δ_{nb}	Δ_{nc}
	($\cdot 10^{-2}$)			($\cdot 10^{-2}$)		
$S_s - S_1$	-0.11	-0.11	-0.11	0.04	-0.11	0.04
$S_1 - S_2$	0.14	0.14	0.14	0.14	0.14	0.14
$S_1 - S_3$	-0.25	-0.25	-0.25	0.04	-0.25	0.04
$S_2 - S_4$	0.04	0.04	0.04	0.19	0.04	0.04
$S_2 - S_5$	**40**	**40**	**40**	**40**	**40**	**40**

Table 5
Frequency values theoretically associated to the paths covered by the travelling waves of mode β originated by a balanced three-phase fault at line L5, and values identified by the CWT analysis.

Path	Length (km)	Theoretical frequency value (traveling wave at light speed) (Hz)	CWT identified frequency value (kHz)	Fault distance error from bus S_s (m)
L1+L2+0.2•L5	4•6	12.3	13.5	553.7
L1+L2+L4	2•7	21.0	25.5	
L1+L3	2•3	49.0	48.5	

Table 6
Frequency values theoretically associated to the paths covered by the travelling waves of mode 0 originated by a phase-to-ground fault at line L5, and values identified by the CWT analysis.

Path	Length (km)	Theoretical frequency value (traveling wave at light speed) (Hz)	CWT identified frequency value (kHz)	Fault distance error from bus S_s (m)
L1+L2+0.2•L5	4•6	10.1	12.8	1261.7
L1+L2+L4	2•7	17.3	18.8	
L1+L3	2•3	40.4	37.2	

Some considerations can be drawn from the results presented in Tables 2-6. First of all, method A correctly identifies the line where the transient occurs and computes with a good accuracy the distance between the source and the nearest node. However, values of Δ_{nj} different from zero are found also for non-faulted lines. In our opinion, this is reasonably due to the superposition of direct and reflected waves, which, case by case, modify the voltage waveforms. The impact of this error turns into a reduced sensitivity when computing the distance d. Indeed, when the transient source is located close to a node, the value of the relevant Δ_{nj} could not be $(\Delta_{nj})_{max}$; in such a case the method would not provide correct information. In the shown results, the largest incorrect value of Δ_{nj} is in the order of $0.25 \cdot 10^{-2}$, which corresponds to a resolution $d_{min} = 0.125\% \cdot D_{nk}$. By considering the longest line in the network of Fig. 3 (line between S_2 and S_5), it is $d_{min} \approx 6$ m. However, by considering the effect of the uncertainty associated with the time stamp provided by the GPS-based device, which turns approximately into an expanded uncertainty

$U(d) = 3 \cdot u_c(\mathrm{d}) \approx 180$ m, it results $d_{min} << U(d)$. Of course, one can state that the practical implementation of such a method will be expensive. Presently, the cost can be estimated in about 7-8,000 Euro for each unit, mainly due to three wide-band voltage-to-voltage transducers and the GPS receiver. However, these costs are expected to decrease in the near future.

As far as method B is concerned, it correctly identifies the faulted line but the accuracy on the fault location is not completely satisfactorily, even if the uncertainty on the identified frequency (about 2% [12], which corresponds to 150 m) is taken into account. This is due to two main reasons: a) the mother wavelet chosen; b) the use of a single-point measurement system. Indeed, it is well known that the results of a wavelet analysis are strictly related to the chosen mother wavelet and the Morlet function probably is not the best option for this application. The use of the information provided by more than one measurement point could improve the accuracy of the method.

5. Conclusions

Two methods for fault location in power distribution networks have been reviewed and compared, by means of EMTP simulations for the case of a typical medium voltage network configuration.

The complementary characteristics of the two considered methods suggests the analysis of a hybrid approach based on the combined use of the two types of information, i.e. starting time and wavelet analysis of voltage transients recorded at some location.

In particular, for the typical configuration of medium voltage networks characterised by a long main feeder and a certain number of short laterals, two measurement units, located at the beginning and at the end the main feeder, may be sufficient. Method A locates the lateral where the fault occurs whereas method B could be applied in order to estimate its location on the identified lateral.

For the specific case of Figure 3, and for the case of a three-phase short circuit in L3, by using only units S_s and S_5, method A identifies a fault at 2003 m away from S_s. This position corresponds to the point where lateral L3 starts (2000 m away from S_s). The information obtained from method A indicates also that, among the various distance values identified by method B (applyied to the transient recorded at S_s), the one that should be considered in this case is 2450.8 m. The fault location is then estimated at about 450 m away from the begin of L3.

This hybrid approach would result in a fault location system less expensive than method A and more efficient than method B.

REFERENCES

[1] M. S. Sachdev, R. Agarwal, "A technique for estimating transmission line fault locations from digital impedance relay measurements", *IEEE Trans. on Power Delivery*, vol. 3, n. 1, pp. 121-129, January 1988.

[2] K. Srinivasan, A. St.-Jacques, "A new fault location algorithm for radial transmission lines with loads", *IEEE Trans. on Power Delivery*, vol. 4, n. 3, pp. 1676-1682, July 1989.

[3] A. A. Girgis, D. G. Hart, W. L. Peterson, "A new fault location technique for two- and three-terminal lines", *IEEE Trans. on Power Delivery*, vol. 7, n. 1, pp. 98-107, January 1992.

[4] G.B. Ancell, N.C. Pahalawatha, "Maximum likelihood estimation of fault location on transmission lines using travelling waves", *IEEE Trans. on Power Delivery*, vol. 9, n. 2, pp. 680-689, April 1994.

[5] O. Chaari, M. Meunier, F. Brouaye, "Wavelets: a new tool for the resonant grounded power distribution systems relaying", *IEEE Trans. on Power Delivery*, vol. 11-3, pp. 1301-1308, July 1996.

[6] F. H. Magnago, A. Abur, "Fault location using wavelets", *IEEE Trans. on Power Delivery*, vol. 13, n. 4, pp. 1475-1480, October 1998.

[7] D.W.P. Thomas, R.E. Batty, C. Christopoulos, A. Wang, "A novel transmission-line voltage measuring method", *IEEE Trans. on Instrumentation and Measurement*, vol. 47, n. 5, pp. 1265-1270, October 1998.

[8] S. Ebron, D.L. Lubkeman, M. White, "A neural network approach to the detection of incipient faults on power distribution feeders", *IEEE Trans. on Power Delivery*, vol. 5, n. 2, pp. 905-914, April 1990.

[9] Z Chen, J.-C Maun, "Artificial neural network approach to single-ended fault locator for transmission lines", *IEEE Trans. on Power Systems*, vol. 15, n. 1, pp. 370-375, February 2000.

[10] N. Kandil, V.K. Sood, K. Khorasani, R.V. Patel, "Fault identification in an AC-DC transmission system using neural networks", *IEEE Trans. on Power Systems*, vol.7, n. 2, pp. 812-819, May 2002.

[11] L. Peretto, R. Sasdelli, E. Scala, R. Tinarelli, "A distributed measurement system for locating transient-voltage sources", *Proc. of the 23rd IEEE IMTC/06*, Sorrento (Italy), April 2006, pp. 1233-1238.

[12] A. Borghetti, S. Corsi, C.A. Nucci, M. Paolone, L. Peretto, R. Tinarelli, "On the use of continuous-wavelet transform for fault location in distribution power networks", *Proc. of the 15th Power System Computation Conference - PSCC 2005*, Liege, Belgium. Selected for publication on the Int. Journal on Electrical Power and Energy Systems, 2006.

[13] L. Peretto, P. Rinaldi, R. Sasdelli, R. Tinarelli: "A System for the Measurement of the Starting Instant of Impulsive Transients", *Proc. of the 21st IEEE IMTC/04*, Como (Italy), May 2004, vol 2, pp. 1394-1398.

[14] L. Angrisani, P. Daponte, M. D'Apuzzo, "Wavelet network-based detection and classification of transients", I*EEE Trans. on Instrumentation and Measurement*, vol. 50, n. 5, October 2001, pp. 1425 – 1435.

[15] P. Goupillaud, A. Grossmann, J. Morlet, "Cycle-octave and related transforms in seismic signal analysis"', *Geoexploration*, 23, 85-102, 1984-1985.

[16] I. Daubechies, "The wavelet transform, time-frequency localization and signal analysis", *IEEE Trans. on Inf. Theory*, vol.36, No.9, pp.961-1005, Sept. 1990.

[17] I. Daubechies, "Orthonormal bases of compactly supported wavelets", *Comm. on Pure and Applied Math.*, vol.XLI, pp.909-996, 1988.

[18] S. G.Mallat, "A theory for multiresolution signal decomposition: the wavelet representation", *IEEE Trans. on PAMI*, vol.11, No.7, pp. 674-693, July 1989.

[19] S.G. Mallat, "Multifrequency channel decompositions of images and wavelet models", *IEEE Trans. on Acoustics. Speech. and Signal Processing*, vol.37, No.12, pp. 2091-2110, December 1989.

[20] O. Rioul, M. Vetterli, "Wavelets and signal processing", *IEEE Signal Processing Magazine*, pp.14-38, October 1991.

[21] J. Mahseredjian, S. Lefebvre and X.-D. Do, "A new method for time-domain modelling of nonlinear circuits in large linear networks", *Proc of the 11th Power Systems Computation conference (PSCC)*, Vol. 2, August 1993, pp. 915-922.

[22] J. Mahseredjian, L. Dubé, L. Gérin-Lajoie, "New advances in the Simulation of Transients with EMTP: Computation and Visualization Techniques", *Electrimacs*, 19 August 2002.

[23] E. Clarke, "Circuit Analysis of A-C Power Systems", vol. 1. New York: John Wiley & Sons, 1943.